Accuracy improve methods for magnetoelectric converter based scanning system.

SUBBOTIN DMITRII
Department of Electrotechnics and Precision Electromechanical Systems
University ITMO
197101, Saint Petersburg, Kronverkskiy pr., 49
RUSSIAN FEDERATION
e-mail: Subb-Dm@yandex.ru

SERGEY LOVLIN
Department of Electrotechnics and Precision Electromechanical Systems
University ITMO
197101, Saint Petersburg,Kronverkskiy pr., 49
RUSSIAN FEDERATION
e-mail: seri-l@yandex.ru

MADINA TSVETKOVA
Department of Electrotechnics and Precision Electromechanical Systems
University ITMO
197101, Saint Petersburg,Kronverkskiy pr., 49
RUSSIAN FEDERATION
e-mail: madina1986@bk.ru

Abstract: - The performance of reversible magneto electric converter based scanning system primarily depends on the control system, which performance is provided in turn by reliability of the real object and the mathematical model used for the calculations, and the reference signal. The article describes a mathematical model of the two-mass reversible scanning mechanism, its comparison with the real system and provides a procedure for constructing an algorithm for defining the inertial reverse scanning device input signal.

Key-Words: - Two-mass mechanism, magnetoelectric converter, reversible scanning device, mathematical model, input assignment, reference signal, setting device.

1 Introduction

Along with widespread of the irreversible scanning devices, which are continuous rotation scanning item [1], in modern technology commonly use reversible scanning devices in which the scanning element can perform fairly complex of reciprocating linear or rotational movement. Such devices are used, for example, at 3D buildings and structures printing, laser scanning systems, multi-axis processing centers, scanning thermal imager systems [2, 3]…

Currently, almost all scanning systems, using reverse converters, based on the operation principle of work with reflected emission (thermal, laser, etc.), which can significantly reduce the size of the rotating parts, and as a result, to reduce the transducer shaft inertia moments.

There are, however, systems where operation with the reflected signal is not possible and it is necessary to place the receiver (emission source), which has a large mass and inertia, directly on the motor shaft. This leads to a significant increase in the oscillatory of the system, inability to use traditional configuration method and the need for a specific converter.

An example of such irreversibly scanning device is contactless magnetoelectric converter (MEC), based on PMSM with high coercivity permanent magnets. MEC proportionally converts an input electrical signal (voltage) to angular movement of its rotor.

Such scanning devices performance is mostly provided by the performance of the control system, which in turn is provided by reliability of the mathematical model of the real object used for the calculations and the quality of reference signal.

The article considers the specially created engine with a limited rotation angle designed for a three-axis infrared telescope scanning axis.

Currently there is no mathematical description of the MEP-mechanism system that takes into account

the features of two-mass object. Thus the considered engine with executive axis is only some drive and not the part of electric drive control system. Hence there is the necessity of MEC-mechanism system description in the control system object format.

The second task is to formulate an algorithm for the accuracy improving not only for the given object, but also for other similar systems.

On results of research the mathematical model, which allowed to carry out the study of the system by mathematical modeling, as well as methods of control signal setpoint synthesis allowing to increase the input signal tracking accuracy were obtained.

In the study the problem of reference signal track deviation was solved, taking into account, that stiffness of motor and telescope tube connection is low (whole object is presented as two-mass model) and the possibility to place the feedback sensor is only on the first mass (motor shaft).

Recommendations for the further work with the object were given.

2 The "MEC-mechanism" two - mass model

By the operation principle and the main parameters MEC refers to the electrical converters with armature displacement normal to the magnetic field lines in the air gap of the inductor. Simplified MEC design presented in Figure 1.

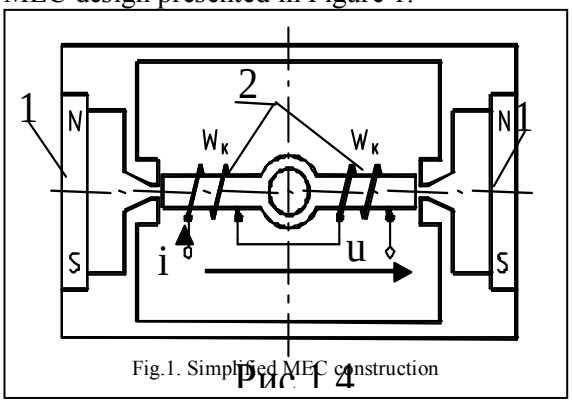

Fig.1. Simplified MEC construction

Рис. 1 д

Polarized MEC functional principle is based on the interaction of magnetic flux magnetizing force, produced by the permanent magnet 1, and the control flow, produced by the current i in the control winding 2 with the coil number W_y, due to the voltage on the control winding u.

This type of construction provides a stable neutral position and also the occurrence of the torque proportional to the value of the angular deviation from the neutral position, directed oppositely to this deviation. Thus, in the absence of coulomb friction torque on the MEC shaft, rotor will tend to return to its initial (neutral) position even without control signal.

Static and dynamic characteristics of MEC with a limited angle rotation for the scan drive are analyzed in [4], synthesis techniques, mathematical models and simulation results for the one-mass speed control system MEC are described in [5, 6]

However, the approach described in [4-6] is applicable only if the stiffness coefficient of the object is high enough. Otherwise, implementation of a control system synthesized this way may provoke fluctuations related with unaccounted slackness and as a result, the inability to achieve the required scan accuracy.

Lack of papers devoted to electric drive control system for scanning devices represented by two-mass models and a small number of papers devoted to direct-drive system lead us to the study of such systems.

According with [7] the dynamics of the MEC can be described by equations:

$$u_y(t) = R \cdot i(t) + L\frac{di}{dt} + Ke \cdot \frac{d\alpha}{dt} \qquad (1, \text{a})$$

$$J\frac{d^2\alpha}{dt^2} + f\frac{d\alpha}{dt} + K_\alpha \cdot \alpha + M_c = K_I \cdot i(t) \qquad (1, \text{b})$$

Where $u_y(t)$ is the control winding of MEC voltage, $i(t)$ is the control winding circuit, R is the control winding resistance, L is the control winding inductance, K_e is the slope of the back-EMF coefficient, J is the total scanning axis inertial torque, f is the inner damping coefficient, M_c is the coulomb friction torque, $K_\alpha = \frac{dM}{d\alpha}$ is the stiffness of mechanical characteristic or «magnetic spring» stiffness, $K_I = \frac{dM}{dI}$ is the stiffness of traction characteristic or electric circuit sensitivity, α is the rotation angle.

Applying Laplace transform to (1, a) and expressing circuit $i(t)$ from (1, a) follows to (2)

$$i(t) = (u_y(t) - K_e \cdot p \cdot \alpha) \cdot \frac{1/R}{T_e \cdot p + 1} \qquad (2)$$

where $T_e = L/R$ – electrical time constant

Applying Laplace transform to (1, b) follows to (3):

$$J \cdot p^2\alpha + f \cdot p \cdot \alpha + K_\alpha \cdot \alpha = M - M_c \qquad (3)$$

where $M = K_i \cdot i(t)$ is the torque provided by MEC

Accepting $d\alpha / dt = p \cdot \alpha = \Omega$ -the angular speed, equation (3) transforms into (4)

This work was financially supported by Government of Russian Federation, Grant 074-U01.

$$J\frac{d\Omega}{dt}+f\cdot\Omega+K_{\alpha}\cdot\alpha=M-M_{c} \quad (4)$$

Hence:

$$\frac{d\Omega}{dt}=(M-M_{c}-f\cdot\Omega-K_{\alpha}\cdot\alpha)\cdot\frac{1}{J} \quad (5)$$

Therefore the two-mass system presented at figure 2 is obtained by combining of block diagram given in [4], equation (5) (where the coordinates of the position α and velocity Ω are considered as speed and position of the first mass), and well-known transfer functions and block diagram of the two-mass mechanism [8].

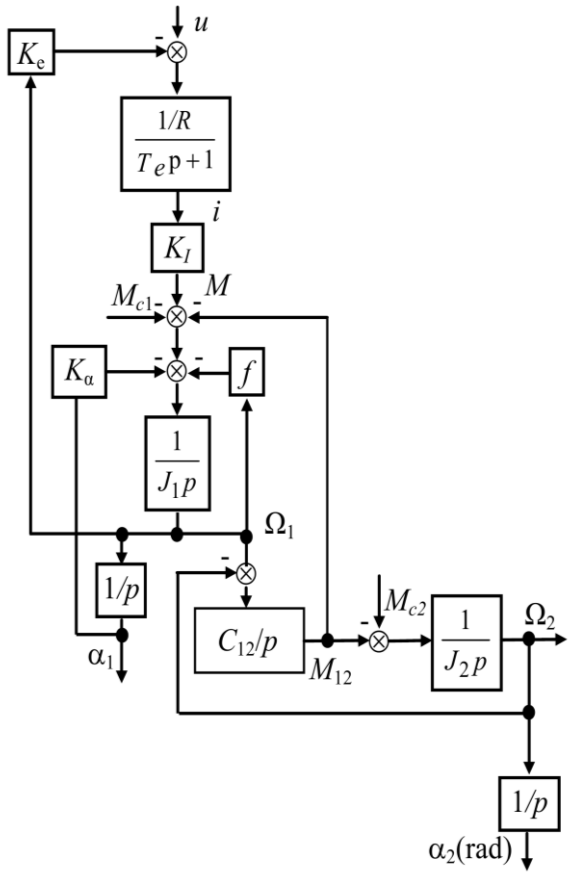

Fig. 2. "MEC-mechanism" two - mass block diagram model

Research of static and dynamic two-mass system characteristics has shown that the transfer functions describing the static properties of the object are not fundamentally different from the transfer functions describing the single-mass model of the system [4]. The differences are only in the order of the numerator and denominator, which is expected taking into account the introduction of additional model integrators.

It should be noted, what there are several state constrains in the system: $u_{\max}(t)\in[-48,48]$, $\alpha(t)\in[-0.5,0.5]$, $\omega_2(t)\in[-1.08,1.08]$ [9]. This constraints are natural feature for many scanning systems. The difference are only in values of given states.

Figure 3 a) shows the Ω_{1m} and α_{1m} first mass angular velocity and rotation angle (curves 1 and 3) and figure 2 b) shows Ω_{2m} and α_{2m} second mass angular velocity and rotation angle (curves 2 and 4) of a two-mass MEC - mechanism model during the transient of 10 V surge control voltage $u_y(t)$ simulation results. The simulation was performed on the basis of the structure depicted on fig. 1 using the parameters of DB600-100-D3043 drive manufactured at the National University "Lviv Polytechnic". In the simulation was used MatLab, Simulink.

Inverter parameters: K_{α} = 4500 N·m/rad; K_I = 85 N·m/A; f = 0; K_e = 1.5 V·s/rad.; L = 0.6 H; R = 14 Ohm; J = 236 kg·m2, M_c = 25 N·m; U_{y_max} = 48 V (maximum voltage of the control winding which is equal to the maximum value of the output voltage of the inverter.). Parameters of the mechanism C_{12} = 3.3·10^6 N·m/rad, J_1 = 18 kg·m^2, J_2 = 218 kg·m^2 are obtained from the developers of telescope rotation device.

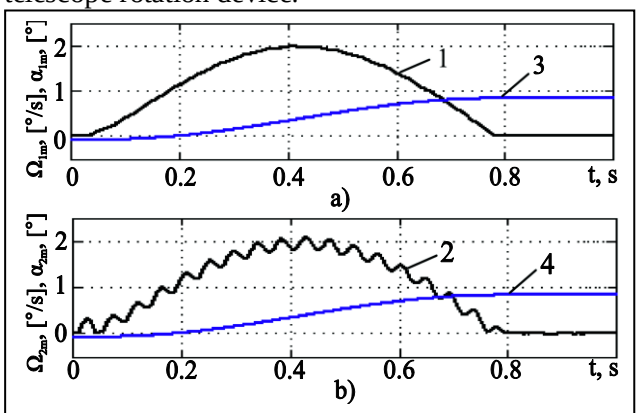

Fig. 3. Electromechanical transients in two-mass model "MEC-mechanism"

3 Comparison with the real object

During the study the comparative analysis of the obtained model and the real object was carried out. The research focuces on the triaxial infrared telescope scan axis.

For the experiment, we used MATLAB Simulink package [10] and the method of direct Simulink coupling with the control object. [11-14]. Figure 4 shows the real object and the mathematical model output values comparing results.

There are several sensors on the real object: the phase current sensors and the position sensors.

Current sensors are integrated in MEC and the position sensors are incremental encoders located on the MEC shaft. The output signal of the sensor is a

position of the rotor. Thus, the position is measured coordinate and speed - is calculated.

During the work it was found that the values of $C_{12} = 3.3 \cdot 10^6$ N·m/rad and $M_c = 25$ N·m does not correspond to reality. The actual values obtained during the experiment are: $C_{12} = 3.1 \cdot 10^5$ N·m/rad and $M_c = 50$ N·m. In the simulation process the simplest model of friction was used.

Figure 4 shows the real object and previously discussed mathematical model output coordinates reaction comparing result for periodic input square wave with 0.4 γ amplitude and 3 sec period duration. On Figure: 1 - real object speed curve Ω_1, 2 – two-mass model first mass speed curve Ω_{1m}, 3 - real object angle curve α_1, 4 - two-mass model first mass angle curve α_{1m}. The second mass speed and angle coordinates aren't presented on the chart because only first mass coordinates can be obtained from the real object.

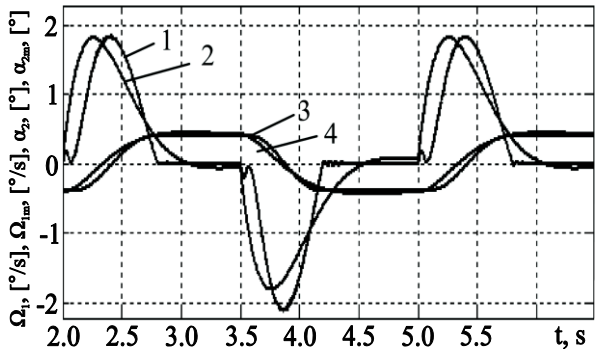

Fig. 4. Electromechanical transients in two-mass model "MEC-mechanism"

Comparative analysis wasn't limited by presented graph, showed that the obtained two-mass mathematical model accurately reflects transient and quasi-stationary modes of the real "MEC - Mechanism" system and can be used for further control system synthesis.

4 Reference signal description

As has been said, the quality of control system performance is related with the quality of reference signal. As an example of specifying reference signal for scanning systems could serve the trapezoidal signal presented in Figure 5.

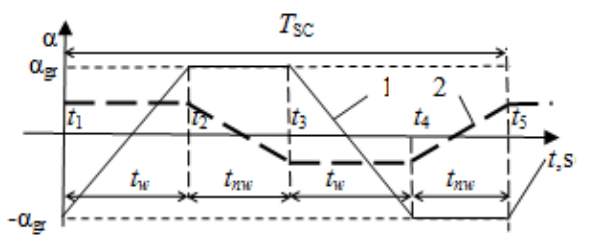

Fig. 5. Electric drive scanning diagram

On Figure: 1 and 2 - curves corresponding to the drive scan diagram by angle and speed, respectively.

Full scan cycle T_{sc} contains two working stroke plot (t_1-t_2 and t_3-t_4) with duration t_w and two nonworking stroke (t_2-t_3 and t_4-t_5) with duration t_{nw}. At working stroke sections angle should vary linearly within the range of $-\alpha_{gr}$ up to $+\alpha_{gr}$ with an acceptable speed maintain error rate Δ%. Angle change principle in nonworking stroke areas are not limited. Duration of nonworking stroke is measured between the end of one working stroke and the beginning of the next.

One of the basic requirements for scanning signal playback is speed maintain high accuracy in working stroke areas of scanning diagram in conditions of limited ultimate performance of Converter, significant coulomb friction value and restrictions on allowable voltage for control winding.

Currently, a widespread practice is to use Simulink-models in real time to control the real objects. For this reason, develop a setting device, which will provide a desired reference signal, in the Simulink expansion.

5 Setting device design

In the case of large reversible mass is usually not allowed to have surges in the acceleration program trajectory, acceleration program trajectory should be a continuous function of time. In this case it is advisable to take a stepwise change of the acceleration derivative to ensure object accelerated revers for a non-working period of time t_{nw}. The object rotation angle change program in this case will result from the triple integration of the acceleration derivative. The simulink based setting device modeling scheme is shown in Figure 6.

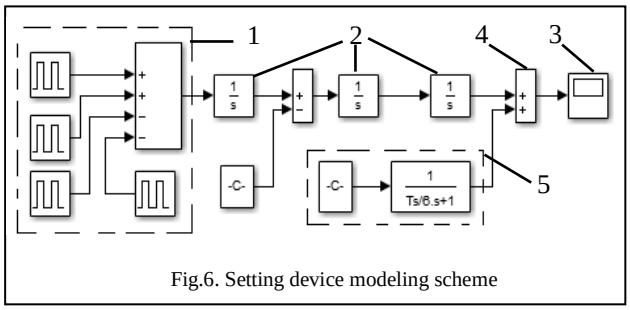

Fig.6. Setting device modeling scheme

On Figure: 1 – acceleration derivative generation unit through the sum of the rectangular input impacts, 2- integrators to produce a consistent graph of angle change, 3- angle measurement output unit, 4- the last integrator output result displacement unit, symmetrically to the time axis by adding a constant, 5- offset ensures zero offset value of acceleration at all reference signal working strokes.

Graph of the third reference variable derivative is shown in Figure 7. In this figure the time points have different values from values on Fig.5. Namely:

$$t_1 = \frac{t_{nw}}{2}, t_2 = t_w + \frac{t_{nw}}{2}, t_3 = t_w + t_{nw}, t_4 = t_w + 1.5t_{nw},$$

$$t_5 = 2t_w + 1.5t_{nw}, t_6 = 2(t_w + t_{nw}).$$

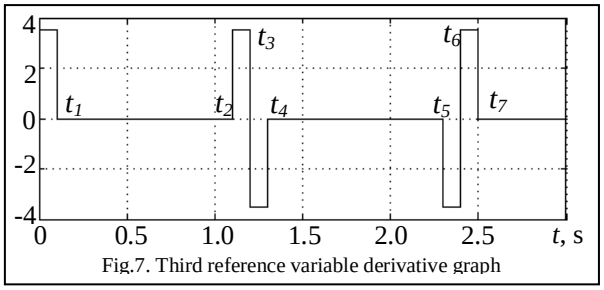

Fig.7. Third reference variable derivative graph

Starting time of a periodic function on Fig.6 coincides with the half of nonworking stroke of reference signal. The reason for this choice is due to the desire for zero initial speed during the system start. For zero average value of the acceleration is necessary to select the negative initial value of acceleration as shown in Fig.8.

Acceleration gap at start-up (Fig. 8) does not lead to a spike in system voltage reference due to the special form of the initial portion of predefined functions, which will be discussed later. Pulse amplitude of the third reference derivative also will be defined later.

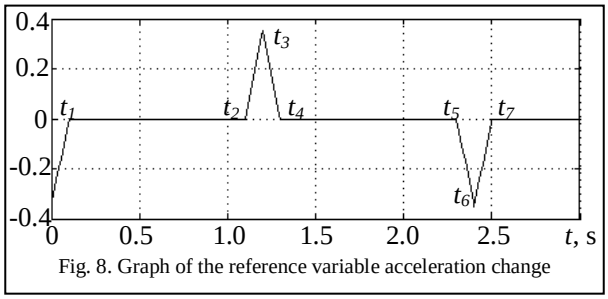

Fig. 8. Graph of the reference variable acceleration change

The graph on Fig. 8. shows that the acceleration at the time $t > 0$ is a continuous function of time, as is required for the control object with high inertia. During the interval $0 < t \le t_1$ the acceleration is negative and increases to zero. Therefore, the speed (Fig. 9) decreases from zero to the nominal value by a quadratic curve. At the time t_1 the acceleration is zero, so the slope of the second order tangent curve is zero and there is no speed graph kink in the moment of transition to the work area. This property is essential to reduce the magnitude of the control voltage surges in the control system.

The method and rate of acceleration and speed change is clear from Fig.8. and Fig.9. Further processes flow must be understood by the given charts.

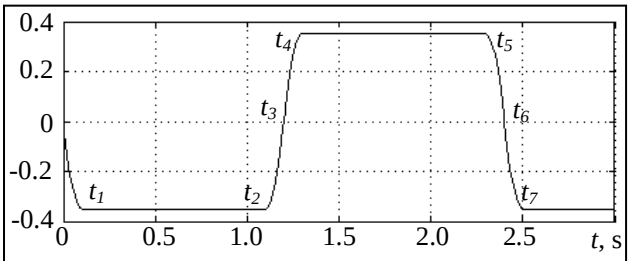

Fig.9. Reference signal speed change graph.

The reference signal graph shown in Fig.10. is obtained by integrating the speed graph, Fig.9. Input graph should be symmetric with respect to the time axis, so the result of the last integrator integrating on Fig. 6. must be moved up by adding a constant. To eliminate the reference signal surges in start-up moment, the constant bias is supplied through aperiodic link with a small time constant. As a result, the initial value of the reference variable is equal to zero, and a constant offset increases smoothly. After the time approximately equal to the half of the reference signal period, the signal graph takes the required form.

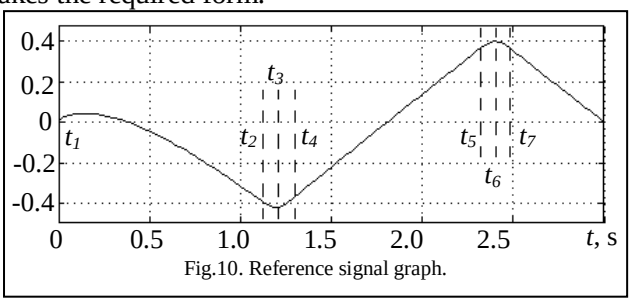

Fig.10. Reference signal graph.

Perform the parameters calculation of the setting device, which scheme is shown in Figure 5. According to the technical specification the nominal speed value in the work stroke is equal to:

$$\Omega_n = \frac{2\alpha_{gr}}{t_w}. \quad (6)$$

Denote the pulse amplitude of the third reference signal derivative on Fig.10. as a_3. Then the acceleration during a time interval $0 < t \le t_1$ with zero initial conditions will vary according to the expression

$$a_2 = a_3 t. \quad (7)$$

The speed on the same interval with zero initial conditions varies according to the expression:

$$a_1 = a_3 \frac{t^2}{2}. \quad (8)$$

The reference signal change law in this interval under the same conditions will be:

$$a = a_3 \frac{t^3}{6}. \quad (9)$$

Within the half of the nonworking stroke angular velocity must vary from zero to the nominal.

Substituting in (8) instead of t the value $0.5t_{nw}$ obtain: $\Omega_n = a_3 \frac{t_{nw}^2}{8}$.

Hence we find the pulse amplitude of the third reference derivative: $a_3 = \frac{8 \cdot \Omega_n}{t_{nw}^2}$.

Using (6) finally obtain the third reference derivative pulses amplitude:

$$a_3 = \frac{16\alpha_{gr}}{t_p t_{nw}^2}. \quad (10)$$

Relative duration of all pulses (signal ratio) is

$$T_{SC} = \frac{t_{nw}}{2T_c} 100\%. \quad (11)$$

All pulses on Fig.7. have a repetition period equal to the T_{SC}. The first pulse has zero delay. The second pulse is delayed with respect to the start time to a time equal to the t_w+0.5t_{nw}, third pulse is delayed t_w+ t_{nw} and finally, the fourth pulse is delayed for a while t_w+1.5t_{nw}. Further graph is repeated with a period of T_{SC}.

A positive value of the third derivative of the reference in the first half of the nonworking stroke would increase the acceleration according to (7) to a value of:

$a_2 = a_3 \frac{t_{nw}}{2}$ or, in view of (10):

$$a_2 = \frac{8 \cdot \alpha_{gr}}{t_w t_{nw}}. \quad (12)$$

But the acceleration of the working range should be zero, so the output of the first integrator is necessary to shift down by an amount determined by the expression (12). The displacement is performed using the biasing DC signal, as shown in Fig.6. This ensures zero acceleration value in all working strokes and, respectively, strictly constant nominal speed value according to Fig.9.

Calculate the change in the reference signal for the first nonworking interval. Since the acceleration on this half-interval does not begin with a zero value, it varies according to the law:

$$a_2 = a_3 t - \frac{8\alpha_{gr}}{t_w t_{nw}} = \frac{16\alpha_{gr}}{t_w t_{nw}^2} t - \frac{8\alpha_{gr}}{t_w t_{nw}},$$

and the speed will not be determined by the formula (8), it vary according to the law:

$$a_1 = \frac{8\alpha_{gr}}{t_w t_{nw}^2} t^2 - \frac{8\alpha_{gr}}{t_w t_{nw}} t.$$

Integrating this expression, obtain a reference signal change for the first nonworking stroke as:

$$a = \frac{8\alpha_{gr}}{3t_w t_{nw}^2} t^3 - \frac{4\alpha_{gr}}{t_w t_{nw}} t^2.$$

Substituting into this expression t=0.5t_{nw} , obtain the reference signal value to the end of the first nonworking stroke equal to:

$$a = -\frac{2\alpha_{gr} t_{nw}}{3t_w}. \quad (13)$$

In the working stroke $t_1 < t \le t_2$ negative velocity has nominal value, therefore, during this period the setpoint will decreased by an amount equal to -2α_{gr}. However, the reference signal graph must be symmetrical with respect to time axis, so the last integrator output must be moved by an amount equal to the module (13) and α_{gr} sum, i.e. by the amount:

$$a_{sum} = \frac{2\alpha_{gr} t_{nw}}{3t_w} + \alpha_{gr}.$$

Constant bias is entered via aperiodic link with a small time constant, Fig.6. This affects the setting device only at the start, eliminating the reference signal surges, as shown in Fig.10.

Formed in this manner reference signal provides exact speed and angle of the scanning element in the scan diagram working strokes.

6 Conclusion

During the research two-mass "MEC - mechanism" mathematical model was obtained and simulation of the transient and quasi-stationary modes of the studied system with high accuracy are made. A comparative analysis of the obtained model and the real object was carried out, which allowed to improve model and its structure affirming parameters.

The resulting mathematical model with noted state constraints allows to describe studied system more accurately and give reasonable approach to the electric scanning devices control system synthesis, that take into account the two-mass object characteristics, by using, for example, optimal control theory methods [15, 16].

Setting device proposed algorithm allows to desine an adjuster, which will provide desired reference signal, taking into account the technical assignment. It also allows to exclude the input signal surges in start-up moments and provides exact speed and angle of the scanning element in the scan diagram working strokes.

By further research and modernization of the system may be to build a control system using fuzzy logic or autotunning systems with robust regulator [17-20]. Such studies may be particularly relevant

because of the influence on the considered object significant wind loads, as well as the drift of the parameters associated with different climatic conditions of the object operation.

References:

[1] U. Samarin Scientific bases and methods of prepress systems terminal devices designing, Moscow state University of printing, Moscow, Russsian Federation, 2004, p. 514.

[2] http://www.riegl.com/ // Riegl - laser measurment systems/15.05.2014.

[3] http://flir.com/ // FLIR - The World Leader in the Design, Manufacture and Marketing of Thermal Imaging Infrared Cameras / 15.05.2014.

[4] Subbotin D.A., Lovlin S.Y., Tsvetkova M.H. Two-mass mathematical model of magnetoelectric converter for reversible scanning device. Manufacturing Engineering, Automatic Control and Robotics: Proceedings of the 14th International Conference on Robotics, Control and Manufacturing Technology (ROCOM '14). 2014. No. 32. pp. 11-14.

[5] Subbotin D.A., Lovlin S.Y., Tsvetkova M.H. Simple speed-maintain control system for reversible scanning device. Advances in Automatic Control: Proceedings of the 16th International Conference on Automatic Control, Modeling & Simulation (ACMOS '14). 2014. No. 35. pp. 87-92

[6] Subbotin D.A., Lovlin S.Y., Tsvetkova M.H. Astatic speed control system for triaxial telescope scanning axis. Advances in Automatic Control: Proceedings of the 16th International Conference on Automatic Control, Modeling & Simulation (ACMOS '14). 2014. No. 35. pp. 175-180

[7] E. Reshetnikov, Y. Sablin, Electromechanical transducers and gas hydraulic actuators, Mashinostroenie, Moscow, Russian Federation, 1964, p.144.

[8] J. T. Tou, Modern control theory, McGraw-Hill, New York, USA, 1971. p. 427.

[9] Md Haider, Ali Biswas, Necessary conditions for optimal control problems with and without state constraints: a comparative study, WSEAS Transactions on Systems and Control, vol. 6, 2011, pp. 217-228.

[10] Computer and Simulation in Modern Science (Volume V), WSEAS Press, 2011.

[11] Shariman Abdullah, Musa Mailah, Collin Tang Howe Hing (2013), Feedforward Model Based Active Force Control of Mobile Manipulator using MATLAB and MD Adams, WSEAS Transactions on Systems, vol. 12, pp. 314-324.

[12] Gurianov A, Denisov K, Computer program state registration certificate number 2009611420 "Program complex SBPET (telescope electric drive rapid prototyping system)" from 12.09.2009

[13] Martin Sysel, MATLAB/Simulink TCP/IP Communication, WSEAS Recent Researches in Computer Science, Proceedings of the 15th WSEAS International Conference on Computers, 2011, p.71-75.

[14] - S. Staines A., Neri F. (2014). "A Matrix Transition Oriented Net for Modeling Distributed Complex Computer and Communication Systems". WSEAS Transactions on Systems, 13, WSEAS Press (Athens, Greece), 12-22.

[15] Md Haider Ali Biswas, Maria do Rosario de Pinho, A Nonsmooth Maximum Principle for Optimal Control Problems with State and Mixed Constraints - Convex Case, Discrete and Continuous Dynamical Systems, vol. special, 2011, pp.174-183.

[16] Md Biswas, Haider Ali, MdR de Pinho, A variant of nonsmooth maximum principle for state constrained problems, Decision and Control (CDC), 2012 IEEE 51st Annual Conference, IEEE, 2012, pp. 7685-7690

[17] Ahmed. M. Kassem (2013), Fuzzy-logic Based Self-tuning PI Controller for High-Performance Vector Controlled Induction Motor Fed by PV-Generator, WSEAS Transactions on Systems, iss. 1, vol. 12, pp. 22-31.

[18] Vladimír Bobál, Petr Chalupa, Petr Dostál, Marek Kubalcík (2013), Self-tuning Control of Non-linear Servomotor: Standard Versus Dual Approach, WSEAS Transactions on Systems, iss. 6, vol. 12, pp. 304-313.

[19] Camilleri M., Neri F., Papoutsidakis M. (2014). "An Algorithmic Approach to Parameter Selection in Machine Learning using Meta-Optimization Techniques". WSEAS Transactions on Systems,13, WSEAS Press (Athens, Greece), 202-213.

[20] M Papoutsidakis, D Piromalis, F Neri, M Camilleri (2014). "Intelligent Algorithms Based on Data Processing for Modular Robotic Vehicles Control". WSEAS Transactions on Systems, 13, WSEAS Press (Athens, Greece), 242-251.